



ELSEVIER

Contents lists available at ScienceDirect

Mechanism and Machine Theory

journal homepage: www.elsevier.com/locate/mechmt

Research paper

Hamiltonian-path based constraint reduction for deployable polyhedral mechanisms

Yuanqing Gu^a, Xiao Zhang^a, Guowu Wei^{b,*}, Yan Chen^{a,c,**}^a School of Mechanical Engineering, Tianjin University, Tianjin 300350, China^b School of Science, Engineering and Environment, University of Salford, Salford M5 4WT, United Kingdom of Great Britain and Northern Ireland^c Key Laboratory of Mechanism Theory and Equipment Design of Ministry of Education, Tianjin University, 135 Yaguan Road, Tianjin 300350, China

ARTICLE INFO

Keywords:

Deployable polyhedral mechanisms (DPMs)
Multi-loop overconstrained mechanism
Overconstraint reduction
Hamiltonian path
Kinematic equivalence

ABSTRACT

Most of the deployable polyhedral mechanisms (DPMs) are multi-loop overconstrained mechanisms that causes barriers for their applications due to the issues in assembly, operation and control. Yet, constraint reduction for these multi-loop overconstrained mechanisms is extremely challenging in kinematics. In this paper, by introducing the Hamiltonian path to investigate the 3D topological graphs of a group of Sarrus-inspired DPMs, we propose a systematic method for constraint reduction of multi-loop overconstrained DPMs. We demonstrate that through the removal of redundant joints with the assistant of tetrahedral Hamiltonian path, one equivalent simplest topological graph of tetrahedral mechanism is identified as a reduction basic unit. Subsequently, one simplest form of Sarrus-inspired cubic mechanism is obtained by investigating two Hamiltonian paths of its dual octahedron and sequentially arranging basic units. Furthermore, a total of nineteen simplest forms of Sarrus-inspired dodecahedral mechanisms are identified from seventeen Hamiltonian paths of its dual icosahedron. The overconstraints in each simplest Sarrus-inspired DPM are greatly reduced while preserving the original one-degree-of-freedom (DOF) motion behavior. The method proposed in this paper not only lays the groundwork for further research in wider deployable polyhedrons, but also inspires the reduction of other multi-loop overconstrained mechanisms, with potential applications in the fields of manufacturing, architecture and space exploration.

1. Introduction

Deployable polyhedral mechanisms (DPMs) have witnessed flourishing growth in recent years because of their potential applications in robotics, space exploration, structure engineering and so on [1,2]. Most of the DPMs are multi-loop overconstrained mechanisms [3], which are always adopted to construct large deployable structures due to their high stiffness and structural stability [4]. DPMs usually contain large numbers of links and joints, and their clearance and input force will affect the deployment dynamics [5], during which the desired deployment motion should generally be smooth, stable, and controllable [6]. Nevertheless, there is little work on the dynamics of DPMs in addition to the velocity and kinetic energy analysis of Fulleroid reported by Wohlhart [7], and

* Corresponding author at: School of Science, Engineering and Environment, University of Salford, Salford M5 4WT, UK.

** Corresponding author: School of Mechanical Engineering, Tianjin University, Tianjin 300350, China.

E-mail addresses: g.wei@salford.ac.uk (G. Wei), yan_chen@tju.edu.cn (Y. Chen).

<https://doi.org/10.1016/j.mechmachtheory.2023.105563>

Received 18 September 2023; Received in revised form 24 November 2023; Accepted 6 December 2023

Available online 14 December 2023

0094-114X/© 2023 The Author(s).

Published by Elsevier Ltd.

This is an open access article under the CC BY license

(<http://creativecommons.org/licenses/by/4.0/>).

Fulleroid-like DPMs proposed by Xiu [8]. Furthermore, the applications of these mechanisms have encountered barriers in assembly, operation and control due to the large numbers of overconstraints embedded in most of the DPMs. To ensure the motion of the overconstrained mechanisms, the strict overconstrained geometric conditions of links and joints must be satisfied [9]. However, due to the harsh working environment of those deployable structures and the errors in fabrication and assembly, the overconstraints bring additional internal loads that can render those mechanisms immobile and reduce the reliability in the operation of the deployable structure, which cannot be completely overcome simply by improving the manufacturing accuracy [10–12]. Therefore, it is important to reduce or even eliminate the redundant constraints of the original overconstrained mechanisms by designing a less-overconstrained

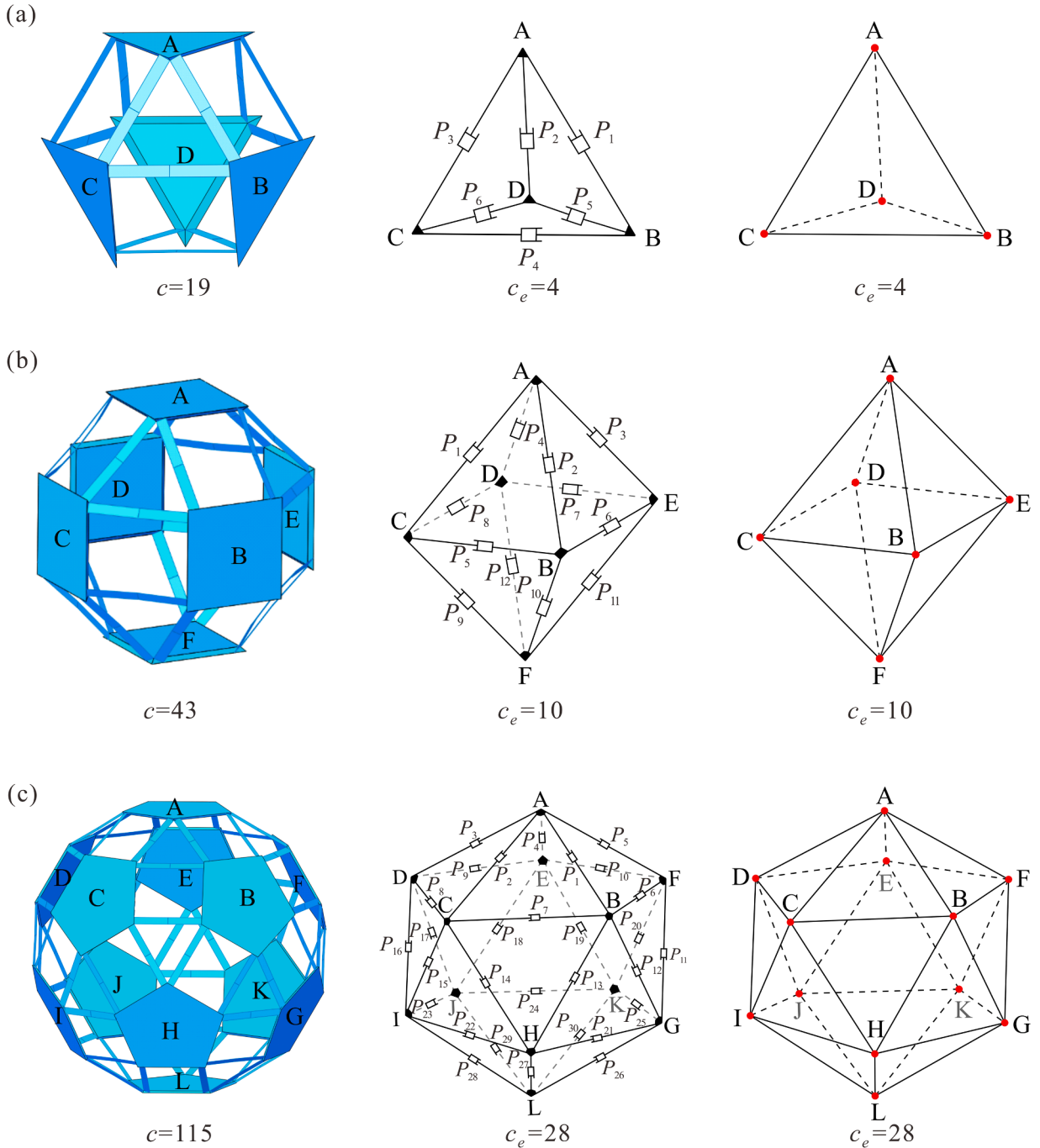


Fig. 1. Sarrus-inspired deployable dodecahedral mechanisms, their equivalent mechanisms with prismatic joints, and the corresponding three-dimensional topological graphs. (a) Tetrahedral mechanism with tetrahedral symmetry, (b) cubic mechanism with octahedral symmetry, and (c) dodecahedral mechanism with icosahedral symmetry.

or non-overconstrained form while keeping their equivalent kinematic behaviors [13,14].

Several constraint-reduction strategies for single-loop and multi-loop mechanisms have been developed. To reduce the degrees of overconstraint in a Bennett linkage, a *RRRS* linkage with kinematic equivalence was reported in [15,16] by using a spherical joint to replace a revolute joint, yet overconstraints still exist in this linkage. Further, Yang et al. [17] proposed a truss method based on Maxwell’s rule [18] to obtain a non-overconstrained form of Bennett linkage as *RSSR* linkage, as well as that of Myard linkage as the *RRSRR* linkage. Yet, there are few works reported on how to reduce the degrees of overconstraint of multi-loop mechanisms while reserving their motion behavior. Based on joint removal with kinematic equivalence, Brown et al. proposed some reduction methods to reduce the redundant constraints of zero-thickness origami-based mechanisms, such as connected one-DOF sections and end-to-end chains [19]. Similar reduction approaches have been applied in the Miura-ori-based deployable array [20]. In addition, the hinge-removing technique [21] was presented for thick-panel origami [22–25] based on construction of Waldron hybrid 6R linkage from two Bennett linkages, which facilitates the engineering application of the thick-panel origami pattern.

Based on three types of one-DOF Sarrus-inspired DPMs developed in our previous work [1], the objective of this paper is to investigate constraint reduction of the proposed multi-loop DPMs. As illustrated in Fig. 1, the tetrahedral, cubic and dodecahedral mechanisms have been constructed in [1], as well as their equivalent mechanisms with prismatic joints and the corresponding three-dimensional topological graphs. By introducing the Hamiltonian path [26] to 3D topological graph and removing redundant constraints, as given in Sections 2 to 4, the simplest constraint forms of these multiloop DPMs are developed to reduce the degrees of overconstraint, respectively, while preserving the original motion behavior including the mobility.

2. Hamiltonian-path based constraint reduction of a deployable tetrahedral mechanism

This section presents the overconstraint reduction of a deployable tetrahedral mechanism by introducing the Hamiltonian path to its 3D topological graph. The procedures of reduction for the tetrahedral mechanism are presented and degrees of overconstraint are analysed to evaluate the reduction results.

2.1. Overconstraint of mechanisms

Based on Grübler-Kutzbach formula [27], the mechanism mobility can be determined by

$$M = d(n - g - 1) + \sum_{i=1}^g f_i, \tag{1}$$

where M is the expected mobility, d is the mobility coefficient and obtained from the motion screw system, n is the number of rigid links and g is the number of kinematic joints, f_i is the degrees of freedom of i th kinematic joints.

Taking the proposed one-DOF deployable tetrahedral mechanism in Fig. 1(a) with 28 links and 36 revolute joints as an example, its expected mobility $M = 6(28 - 36 - 1) + 36 = -18$, hence it is a highly overconstrained mechanism. Thus, the original degrees of overconstraint c [1] in this mechanism can be derived as

$$c = m - M = 1 - (-18) = 19 \tag{2}$$

in which m stands for the actual mobility of the mechanism.

Meanwhile, referring to the equivalent strategy reported in our previous work [1], the equivalent tetrahedral mechanism with six prismatic joints is shown in Fig. 1(a), whose equivalent degrees of overconstraint c_e is

$$c_e = m - M = 1 - (-3) = 4. \tag{3}$$

However, overconstraints still exist. To reduce or even eliminate the overconstraints in multiloop mechanisms and find the effective constraint space for polyhedral platforms, we investigate the reduction process as follows by utilizing the topology operation.

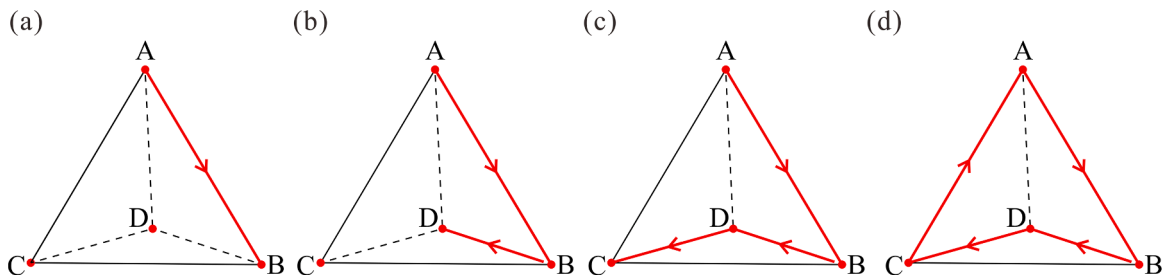


Fig. 2. Only one Hamiltonian path in a tetrahedron.

2.2. Hamiltonian path of a tetrahedral topology graph

It should be pointed out that the essential premise of reduction is that each platform requires at least two equivalent prismatic joints to maintain the close-loop mechanism, i.e., each vertex is related to at least two edges in the topological graph, then the original kinematic properties including mobility and radial motion should be preserved among polyhedral platforms. It is mathematically interesting to find that the Hamiltonian path (or Hamiltonian cycle) [26] matches the premise of the reduction process. There are two significant characteristics of the Hamiltonian path: first, it is a close-loop path with a sequence of edges that visits all the vertices of a graph; second, each vertex between two edges is only accessed exactly once along the path. For demonstration purpose, the generation process of Hamiltonian path in a tetrahedron is taken as an example, see Fig. 2. First, starting from vertex A, any edge among AB, AC and AD is identical due to tetrahedral symmetry, here edge AB in Fig. 2(a) is selected. Subsequently, edges BD and BC are also identical in tetrahedral symmetry, so edge BD is selected in Fig. 2(b). Next, edge DC can only be selected to connect vertex C instead of edge DA, see Fig. 2(c). Finally, the close-loop path is obtained in Fig. 2(d) by connecting the initial vertex A through the edge CA. Note that, due to the tetrahedral symmetry, there is only one Hamiltonian path in a tetrahedron.

2.3. Hamiltonian-path based reduction of the tetrahedral mechanism

The obtained Hamiltonian path, also given in Fig. 3(a), can split the tetrahedron into two half shells, as shown in Fig. 3(b) and (e). On the one hand, the half shell in Fig. 3(b) is an assembly of two one-DOF triangular units ADC and ADB connected by one common edge AD. The constraint matrix in this two-loop equivalent mechanism can be directly derived as

$$M'_{e1} = \begin{bmatrix} S_{f1} & S_{f2} & \mathbf{0} & S_{f5} & \mathbf{0} \\ \mathbf{0} & -S_{f2} & S_{f3} & \mathbf{0} & S_{f6} \end{bmatrix}, \tag{4}$$

in which the detailed calculation of equivalent motion screws S_{fi} can be found in [1].

The actual mobility of this two-loop mechanism shown in Fig. 3(b) is $m = n_e - \text{rank}(M'_{e1}) = 5 - 4 = 1$, and the kinematic behavior of its mapped Sarrus-inspired mechanism is unchanged, in which the detailed analysis can be found in Appendix A. Hence, the edge BC is redundant for its mechanism topology and can be removed without affecting the motion behavior of the polyhedral platforms.

Yet, the degrees of overconstraint of this two-loop equivalent mechanism is $c_e = m - M = 1 - (-3) = 2$, in which further reduction can be explored. Here are five edges AB, BD, DC, CA and AD reserved in Fig. 3(b), then we can only remove edge AD under the mentioned reduction premise due to each vertex should be involved with at least two edges. Thus, a skew quadrilateral (non-planar quadrilateral) ABDC is obtained in Fig. 3(c) (highlighted in blue). The constraint matrix of this single-loop equivalent mechanism with

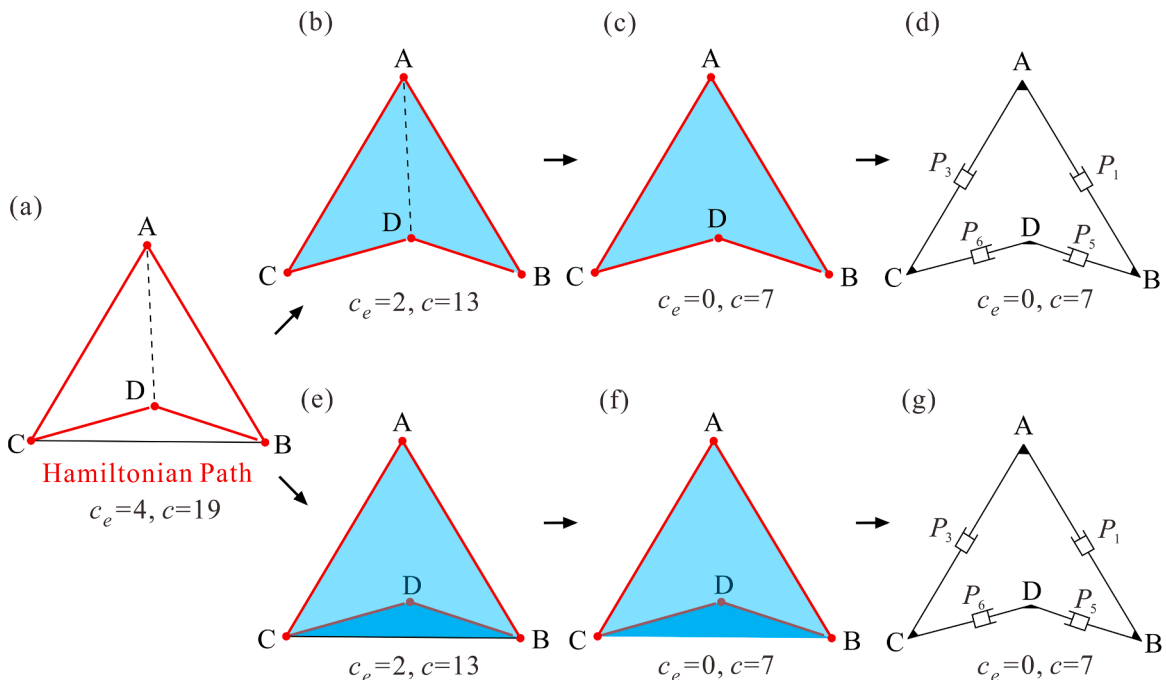


Fig. 3. Reduction process of equivalent tetrahedral mechanism. (a) The only one 3D Hamiltonian path (illustrated in red line); (b) one half shell split by Hamiltonian path, and (c) the simplest topological graph and (d) its corresponding simplest equivalent mechanism; (e) the other half shell and (f) its simplest topological graph and, (g) equivalent mechanism, which are congruent with (b)-(d) respectively. (For interpretation of the references to colour in this figure legend, the reader is referred to the web version of this article.)

four equivalent prismatic joints P_1, P_3, P_6 and P_5 in Fig. 3(d) is

$$\mathbf{M}'_{e1} = [S_{f1} \ S_{f3} \ S_{f6} \ S_{f5}] \tag{5}$$

The mobility of this single-loop mechanism is $m = n_e - \text{rank}(\mathbf{M}'_{e1}) = 4 - 3 = 1$ with its degrees of overconstraint $c_e = m - M = 1 - 1 = 0$, in which its unchanged kinematics is revealed and proved in Appendix A. Therefore, we can regard a skew quadrilateral as the simplest topological graph, i.e., the single-loop mechanism in Fig. 3(d) can be obtained as the simplest constraint form with four equivalent prismatic joints.

On the other hand, the other half shell in Fig. 3(e) is also a one-DOF assembly of two triangular units ABC and BCD connected by edge BC, which is congruent with the one in Fig. 3(b) due to the symmetry. Thus, the same reduction process can be carried out to obtain the simplest topological graph in Fig. 3(f) and the simplest equivalent mechanism in Fig. 3(g), which are identical to Figs. 3(c) and 3(d), respectively.

Ultimately, by mapping the proposed simplest equivalent mechanism in Figs. 3(d) or 3(g) back to the original Sarrus-inspired mechanism, Fig. 4(a) shows the simplified tetrahedral mechanism integrated by four Sarrus linkages, in which the one-DOF synchronized radial motion is preserved, whose prototype is shown in Fig. 4(b). Nevertheless, the actual overconstraints of this simplified Sarrus-inspired mechanism are $c = m - M = 1 - (-6) = 7$ due to the four involved overconstrained Sarrus linkages. Compared with the original mechanism in Fig. 1(a), the actual overconstraints are greatly reduced from 19 to 7. Furthermore, if we remove arbitrary one of eight limbs among four platforms, i.e., remove two links with three revolute joints in a Sarrus linkage, the mobility of this tetrahedral mechanism will become two, hence the simplified tetrahedral mechanism in Fig. 4 can be regarded as the simplest constraint form.

Furthermore, the skew quadrilateral topological graph in Fig. 3(c) will be taken as the basic unit with $c_e = 0$ to conduct the constraint reduction in complex Hamiltonian paths for other polyhedral mechanisms.

3. Constraint reduction of other deployable polyhedral mechanisms

In this section, the constraint reduction processes of deployable cubic and dodecahedral mechanisms are presented by using the obtained skew quadrilateral as the basic unit, in which the original one-DOF radial motion is preserved in each case. As an extension of reduction method, the reduction of a quadrangular prism mechanism is subsequently demonstrated.

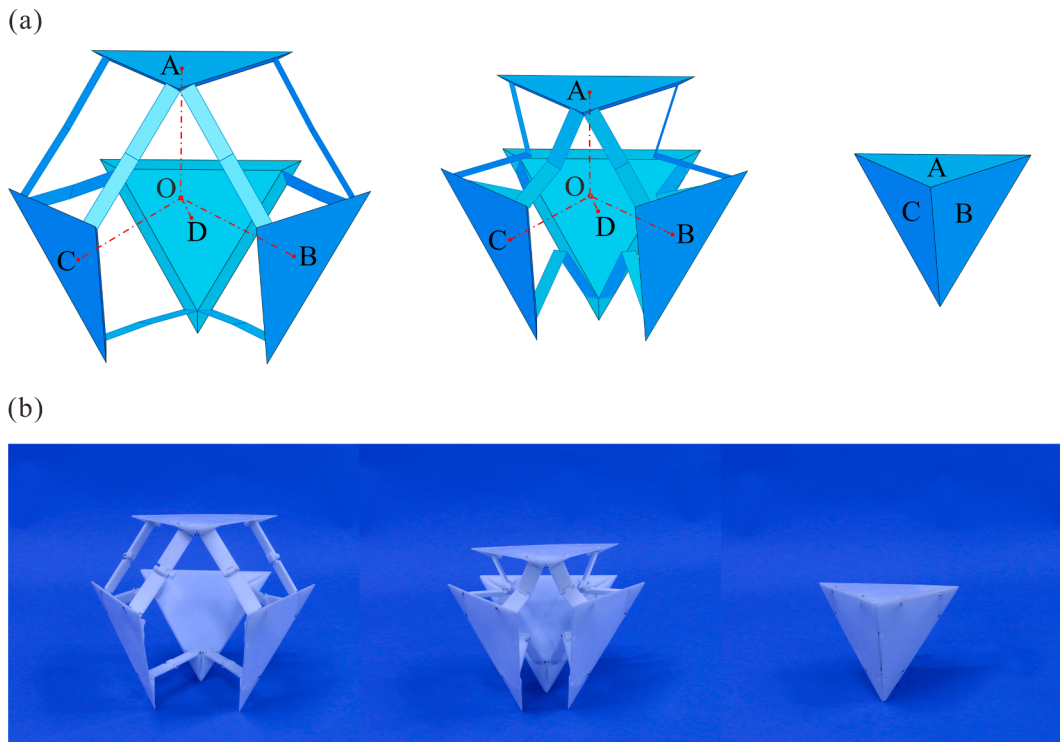


Fig. 4. Motion sequence of the simplest tetrahedral mechanism. (a) CAD model and (b) prototype.

3.1. Constraint reduction of the deployable cubic mechanism

Inspired by the characteristic of the Hamiltonian path that matches the premise of reduction process, the similar topology operation can be carried out to demonstrate the reduction of the deployable cubic mechanism given in Fig. 1(b), in which the original and equivalent overconstraints are $c_e = 10$ and $c = 43$, respectively. Note that, the 3D topological graph of the equivalent cubic mechanism in Fig. 1(b) with a basis of dual octahedron that possesses totally two distinct Hamiltonian paths [28]. First, Hamiltonian path 1 of a double-Z shape in an octahedron is shown in Fig. 5(a) in red lines, it splits this octahedron into two congruent half shells due to the octahedral symmetry, see Fig. 5(b) and 5(d). Taking Fig. 5(b) as an example, this half shell is an assembly of four one-DOF triangular units FBC, BCA, CAD and ADE with equivalent kinematics, the mobility in its corresponding mechanism can be calculated as one with $c_e = 4$ and $c = 25$, which proves that the edges DF, EF and EB are redundant. Subsequently, we can arrange the proposed skew quadrilateral basic unit in this half shell generated from path 1 to conduct the further reduction. As shown in Fig. 5(c), starting from vertex F with a smaller included edge angle, we can arrange a quadrilateral FBAC (highlighted in blue), thus the next quadrilateral ACDE can be readily arranged in the rest space. Compared with the reduction result in Fig. 5(b), we can regard that edges BC and AD are removed, it results in a two-loop one-DOF mechanism constructed by seven equivalent prismatic joints with $c_e = 0$. Meanwhile, due to the octahedral symmetry, the identical reduction result based on the other half shell in Fig. 5(d) can also be obtained, see Fig. 5(e).

According to the topological graph in Fig. 5(c) from path 1, the corresponding equivalent prismatic joints S_{fi} and the constraint graph are given in Fig. 6, in which the detailed calculation about equivalent motion screws can be found in [1]. Its constraint matrix M'_{e2} can be derived as

$$M'_{e2} = \begin{bmatrix} S_{f1} & \mathbf{0} & S_{f3} & S_{f7} & S_{f8} & \mathbf{0} & \mathbf{0} \\ -S_{f1} & S_{f2} & \mathbf{0} & \mathbf{0} & \mathbf{0} & S_{f9} & S_{f10} \end{bmatrix}, \tag{6}$$

where the rank of this matrix is 6, and mobility of the cubic mechanism in Fig. 6 can be verified as $m = n_e - \text{rank}(M'_{e2}) = 7 - 6 = 1$, and the equivalent kinematics can also be revealed based on similar matrix method given in Appendix A.

Yet, the actual overconstraints $c = 13$ still exist in the corresponding Sarrus-inspired mechanism due to the related seven Sarrus

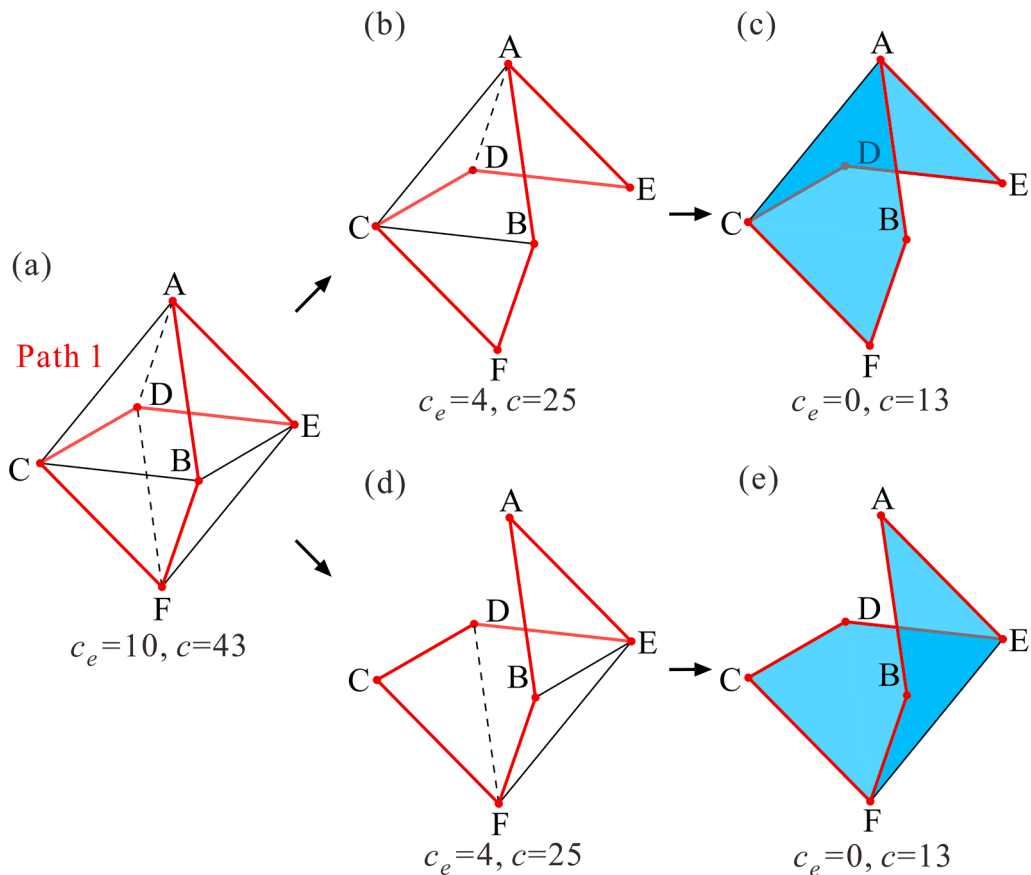


Fig. 5. Reduction process of equivalent cubic mechanism using Hamiltonian path 1. (a) Hamiltonian path 1 in the 3D topological graph, (b) one half shell split by path 1, (c) the simplest topological graph, (d) the other half shell, and (e) its simplest topological graph.

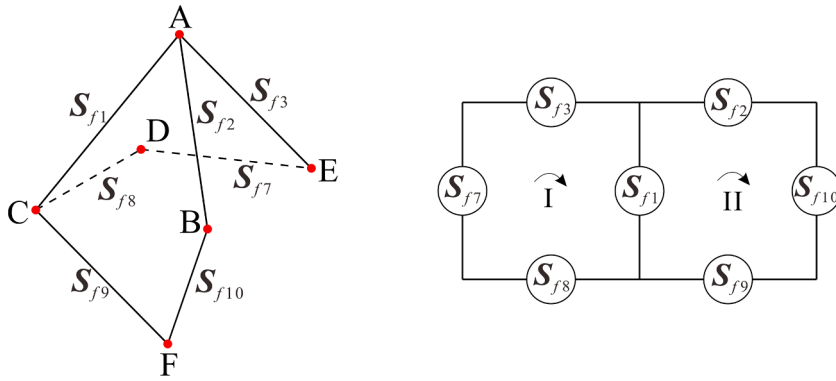


Fig. 6. Constraint graphs of the simplest cubic mechanism derived from path 1.

linkages. Further, if we remove the common edge AC in Fig. 5(c), i.e., S_{f1} in Fig. 6, the single-loop equivalent mechanism with six prismatic joints will occur, then its mobilities will become two, which is contrary to the reduction premise. Thus, the topological graph in Fig. 5(c) or Fig. 5(e) can be identified as the one-DOF simplest constraint path derived from path 1.

On the other hand, Hamiltonian path 2 of a three-fold zigzag shape is given in Fig. 7(a), which also splits this octahedron into two congruent half shells due to the symmetry, see Fig. 7(b) and 7(d). For the topological graph in Fig. 7(b), three external triangular units are connected to the central one, respectively, also leading to a one-DOF four-loop mechanism with $c_e = 4$ and $c = 25$. Next, due to its three-fold symmetry, we can select any one of vertices D, E and F at the beginning to arrange the skew quadrilateral basic unit. For example, a quadrilateral FBAC is generated in Fig. 7(c), yet two resulting triangular units ACD and ABE as illustrated in grey cannot be

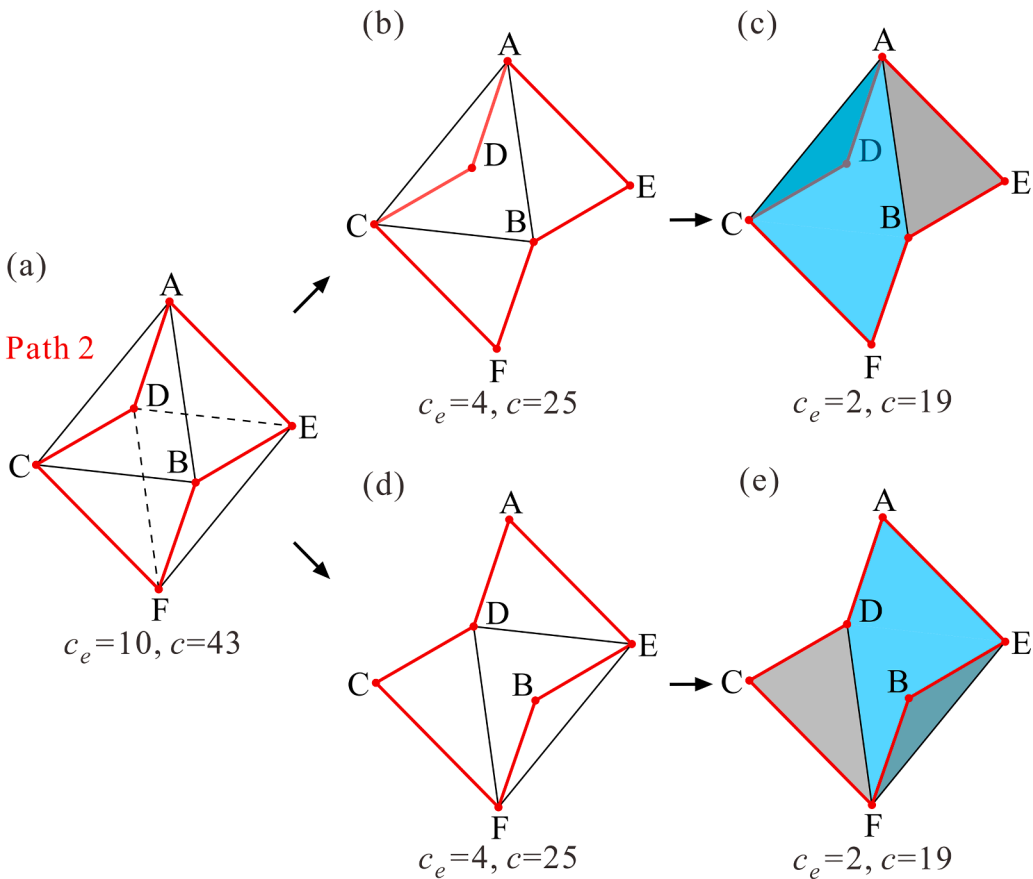


Fig. 7. Reduction process of equivalent cubic mechanism using Hamiltonian path 2. (a) Hamiltonian path 2 in the 3D topological graph, (b) one half shell split by path 2, (c) the simplified topological graph, (d) the other half shell, and (e) its simplified topological graph.

merged into a quadrilateral anyway, which also applies to the identical reduction result in Fig. 7(e). No matter which arrangement for this case, there are always two triangles that cannot be merged.

Referring to the topological graph in Fig. 7(c) from path 2, the corresponding constraint graph is given in Fig. 8 and its constraint matrix M'_{e2} is

$$M'_{e2} = \begin{bmatrix} S_{f1} & 0 & 0 & S_{f4} & 0 & S_{f8} & 0 & 0 \\ -S_{f1} & S_{f2} & 0 & 0 & 0 & 0 & S_{f9} & S_{f10} \\ 0 & -S_{f2} & S_{f3} & 0 & S_{f6} & 0 & 0 & 0 \end{bmatrix}, \tag{7}$$

where the rank of this matrix is 7, and mobility of the cubic mechanism in Fig. 8 is $m = n_e - \text{rank}(M'_{e2}) = 8 - 7 = 1$. As a result, the topological graph in Fig. 7(c) has mobility one with $c_e=2$ and $c = 19$, due to the connection of one skew quadrilateral unit and two triangular units.

However, if edge AB (or AC) is further removed, the mobility will become two. Thus, the constraint path in Fig. 7(c) or Fig. 7(e) can be regarded as the simplified constraint path derived from path 2. Yet, compared with the constraint path in Fig. 5(c), this constraint path cannot be treated as the simplest one of this cubic mechanism due to its eight associated equivalent prismatic joints among all six platforms. Hence, the only one simplest topological graph of the cubic mechanism can be identified in Fig. 5(c) or 5(e).

According to the simplest topological graph in Fig. 5(c), the simplest one-DOF deployable cubic mechanism is obtained with the original motion behavior of its platforms unchanged, whose motion sequences are given in Fig. 9. Compared with original cubic mechanism in Fig. 1(b), the actual overconstraints in this simplest Sarrus-inspired cubic mechanism are greatly reduced from 43 to 13.

In this section, the one-DOF simplest topological graph of the cubic mechanism is identified as two one-DOF skew quadrilaterals connected by one common edge, the reduction method inspired by Hamiltonian path can be readily applied to the complex dodecahedral mechanism in next section.

3.2. Constraint reduction of the deployable dodecahedral mechanism

As given in Fig. 1(c), the original 3D topological graph of the deployable dodecahedral mechanism is related to its dual icosahedron with $c_e = 28$ and $c = 115$. There are totally 17 distinct Hamiltonian paths on an icosahedron [29], which presents a different challenge to find all simplest constraint forms for this mechanism. Nevertheless, the proposed reduction method by arranging the skew quadrilateral basic units can still be conducted for dodecahedral mechanisms.

Taking an arbitrary Hamiltonian path as an example, as shown in Fig. 10(a) in red lines, which connects all twelve vertices without any symmetry. Next, two distinct half shells split by path 1 are generated in Figs. 10(b) and 10(d), respectively, each of which consists of ten one-DOF triangular units connected in sequence and can be regarded as a one-DOF assembly. It is intuitive that we only need to repeat the quadrilateral arrangements as illustrated from Figs. 5(b) to (c) to explore the simplest constraint path. Starting from vertex A in Fig. 10(b), one-DOF skew quadrilaterals ADIC, CILH, CHGB, BGKF and FKJE can be sequentially arranged inside the Hamiltonian path, leading to a one-DOF assembly of these five basic units as shown in Fig. 10(c). Here, the redundant edges CD, IH, BH, FG and EK are removed alternately, and two adjacent basic units share one common edge, i.e., edges CI, CH, BG and FK, respectively. Similarly, as shown in Fig. 10(d), starting from vertex C, if we further arrange five skew quadrilaterals CBFA, AFED, DEJI, IJKL and LKGH in the other half shell, another different simplest constraint path is obtained in Fig. 10(e).

Referring to the first example of the simplest dodecahedral mechanism represented by Fig. 10(c), its mobility can be analyzed and verified with a total of 16 associated equivalent kinematic pairs. Based on the corresponding constraint graph in Fig. 11(a), its related constraint matrix M'_{e3} is

$$M'_{e3} = [M'_{11} \quad M'_{12}], \tag{8}$$

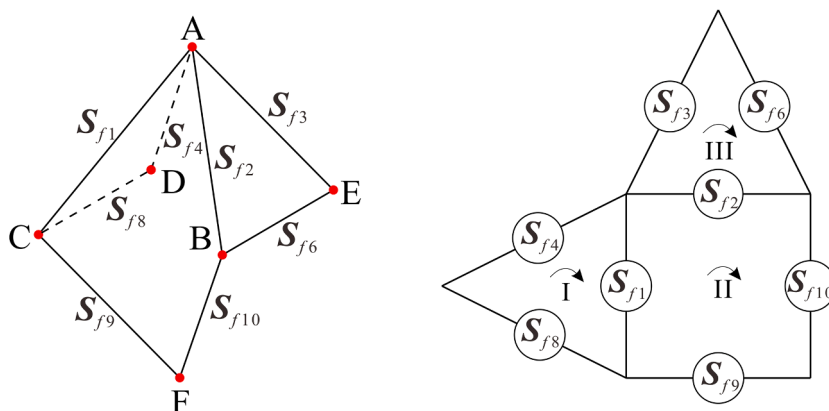


Fig. 8. Constraint graphs of the simplified cubic mechanism derived from path 2.

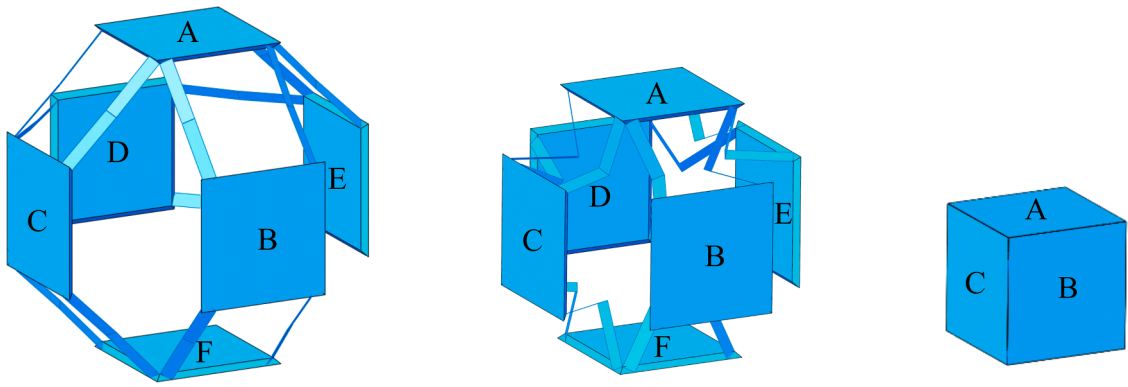


Fig. 9. Motion sequence of the simplest cubic mechanism.

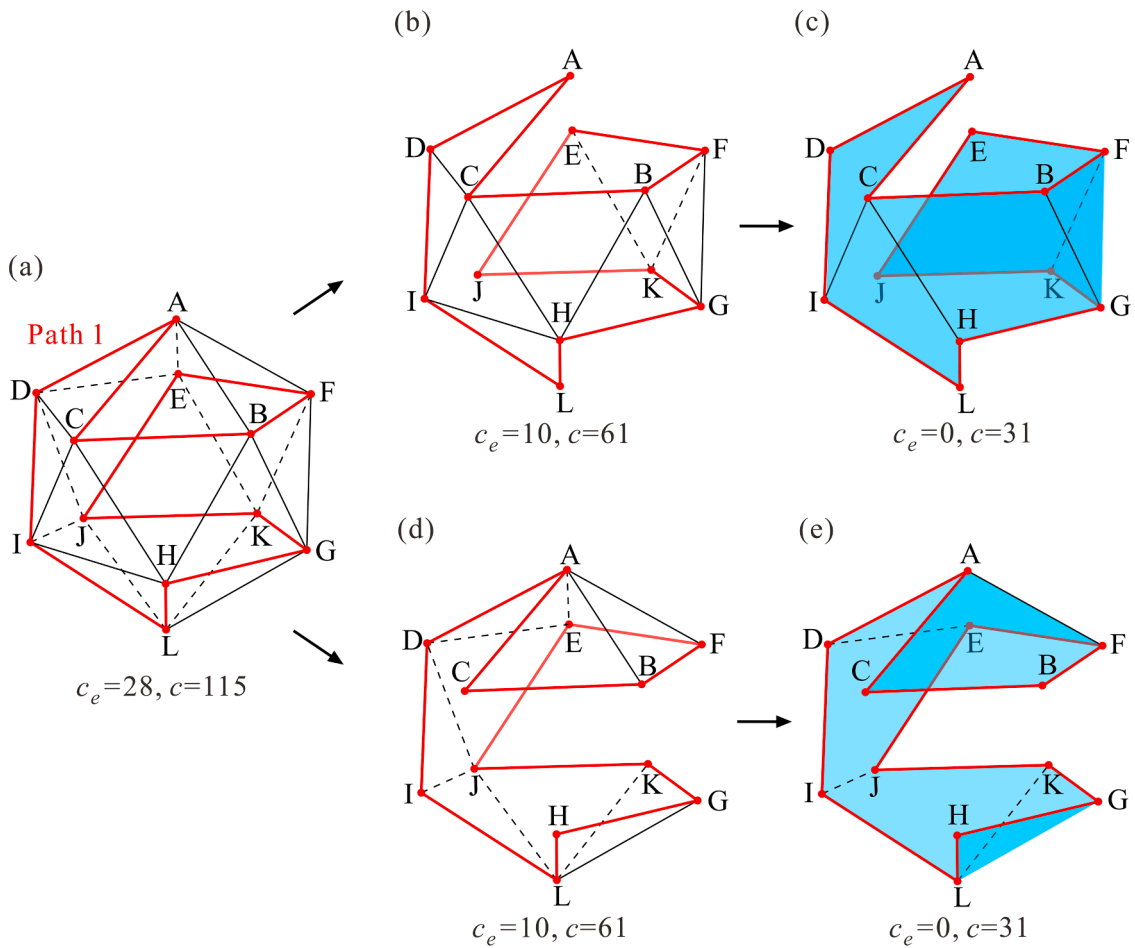


Fig. 10. Reduction process of equivalent dodecahedral mechanism. (a) Hamiltonian path 1 in the 3D topological graph, (b) one half shell split by this path, (c) its simplest constraint path with the removal of redundant edges CD, IH, BH, FG and EK, (d) the other half shell split by this path, and (e) its simplest constraint path with the removal of redundant edges AB, AE, DJ, JL and LG.

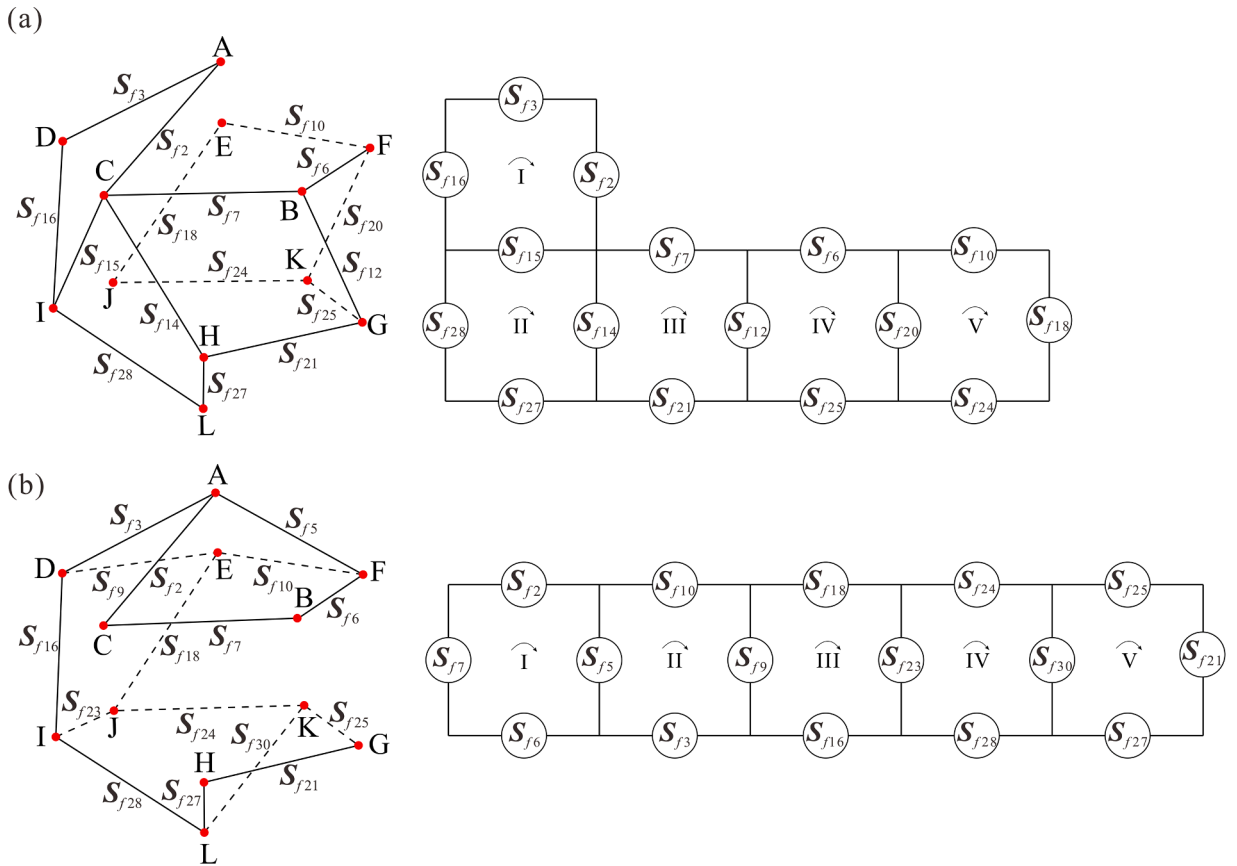


Fig. 11. Constraint graphs of the simplest dodecahedra mechanisms.

with

$$\begin{aligned}
 \mathbf{M}'_{11} &= \begin{bmatrix} S_{f2} & S_{f3} & 0 & 0 & 0 & 0 & 0 & S_{f15} \\ 0 & 0 & 0 & 0 & 0 & 0 & S_{f14} & -S_{f15} \\ 0 & 0 & 0 & S_{f7} & 0 & S_{f12} & -S_{f14} & 0 \\ 0 & 0 & S_{f6} & 0 & 0 & -S_{f12} & 0 & 0 \\ 0 & 0 & 0 & 0 & S_{f10} & 0 & 0 & 0 \end{bmatrix}, \\
 \mathbf{M}'_{12} &= \begin{bmatrix} S_{f16} & 0 & 0 & 0 & 0 & 0 & 0 & 0 \\ 0 & 0 & 0 & 0 & 0 & 0 & S_{f27} & S_{f28} \\ 0 & 0 & 0 & S_{f21} & 0 & 0 & 0 & 0 \\ 0 & 0 & S_{f20} & 0 & 0 & S_{f25} & 0 & 0 \\ 0 & S_{f18} & -S_{f20} & 0 & S_{f24} & 0 & 0 & 0 \end{bmatrix}.
 \end{aligned}$$

The rank of this constraint matrix \mathbf{M}'_{e3} is 15, thus the mobility of this dodecahedral mechanism can be derived as $m = n_e - \text{rank}(\mathbf{M}'_{e3}) = 16 - 15 = 1$.

Then, using the same approach, the constraint graph derived from another different path in Fig. 10(e) is shown in Fig. 11(b), the corresponding constraint matrix \mathbf{M}'_{e3} is

$$\mathbf{M}'_{e3} = [\mathbf{M}'_{11} \quad \mathbf{M}'_{12}] \tag{9}$$

with

$$\mathbf{M}_{11}^r = \begin{bmatrix} S_{f2} & 0 & S_{f5} & S_{f6} & S_{f7} & 0 & 0 & 0 \\ 0 & S_{f3} & -S_{f5} & 0 & 0 & S_{f9} & S_{f10} & 0 \\ 0 & 0 & 0 & 0 & 0 & -S_{f9} & 0 & S_{f16} \\ 0 & 0 & 0 & 0 & 0 & 0 & 0 & 0 \\ 0 & 0 & 0 & 0 & 0 & 0 & 0 & 0 \end{bmatrix},$$

$$\mathbf{M}_{12}^r = \begin{bmatrix} 0 & 0 & 0 & 0 & 0 & 0 & 0 & 0 \\ 0 & 0 & 0 & 0 & 0 & 0 & 0 & 0 \\ S_{f18} & 0 & S_{f23} & 0 & 0 & 0 & 0 & 0 \\ 0 & 0 & -S_{f23} & S_{f24} & 0 & 0 & S_{f28} & S_{f30} \\ 0 & S_{f21} & 0 & 0 & S_{f25} & S_{f27} & 0 & -S_{f30} \end{bmatrix}.$$

The rank of this constraint matrix \mathbf{M}_{e3}^r is 15 and the mobility of this simplest dodecahedral mechanism is also $m = n_e - \text{rank}(\mathbf{M}_{e3}^r) = 16 - 15 = 1$.

Referring to the above mobility analysis, the equivalent mechanism obtained in Fig. 10(c) has mobility of one with equivalent overconstraint $c_e = 0$, as well as the case in Fig. 10(e), hence both can be regarded as simplest constraint paths among the twelve polyhedral platforms. Duo to the two distinct simplest constraint forms are derived from one common Hamiltonian path 1 in Fig. 10(a), they have identical outer contour lines so that they can be called complementary simplest paths.

Ultimately, by mapping the simplest topological graphs in Fig. 10(c) and 10(e) to the original Sarrus-inspired mechanism, two simplest dodecahedral mechanisms that preserve original one-DOF radial motion are generated in Fig. 12, in which kinematic equivalence can also be proven based on the matrix method as given in Appendix A. Compared with the original dodecahedral mechanism in Fig. 1(c), the degrees of overconstraint in these simplest mechanisms are greatly reduced from 115 to 31.

In addition to the above Hamiltonian path 1 as given in Fig. 10(a), some other distinct Hamiltonian paths on a dual icosahedron can also be utilized to identify the simplest dodecahedral mechanisms, which is organized and listed as follows.

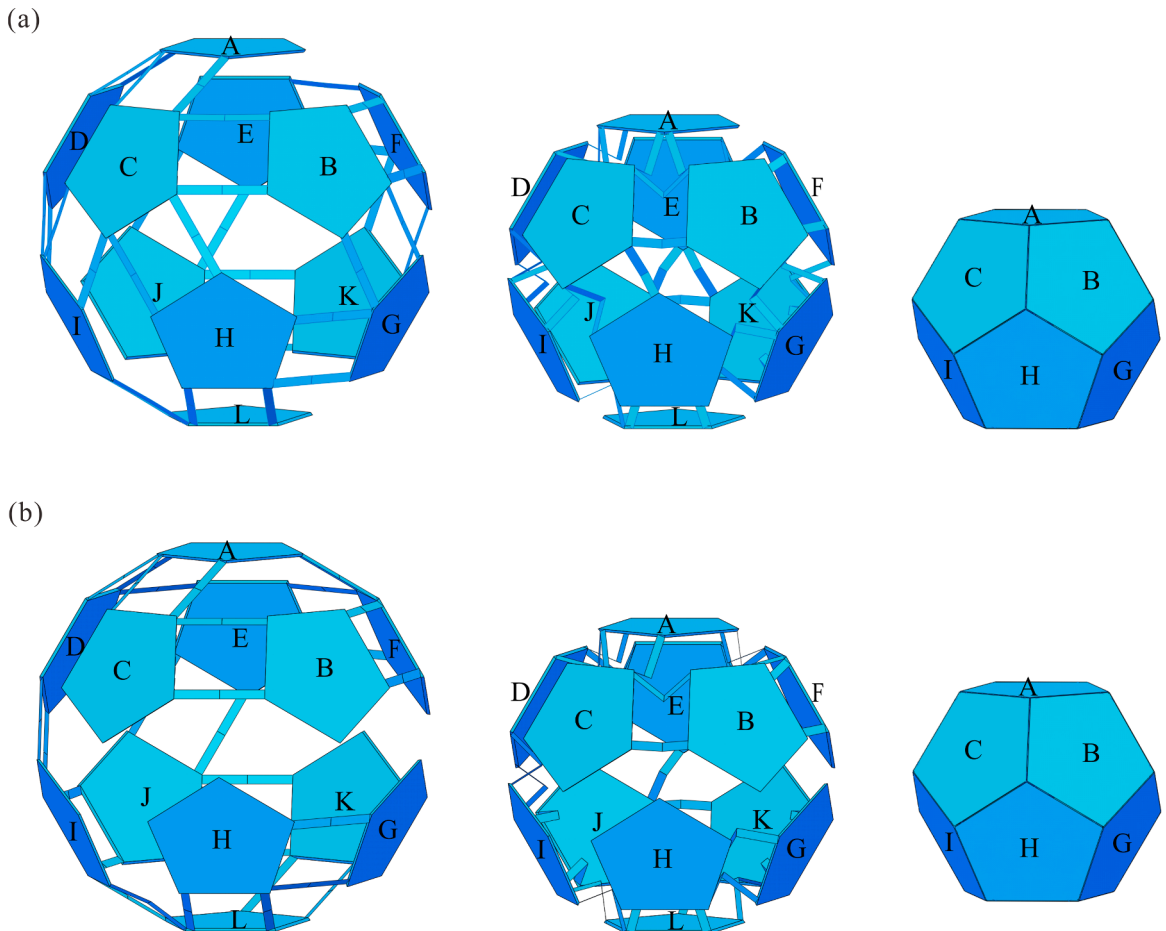


Fig. 12. Motion sequence of the simplest dodecahedral mechanisms obtained from (a) one half shell and (b) the other one.

Table 1
Reduction results of dodecahedral mechanism using paths 1 to 5.

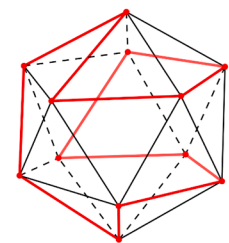
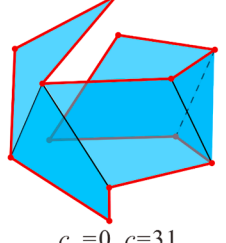
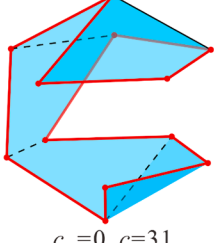
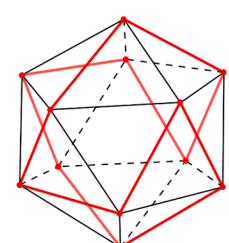
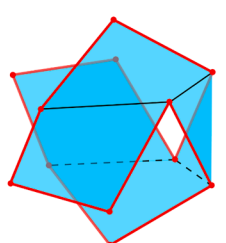
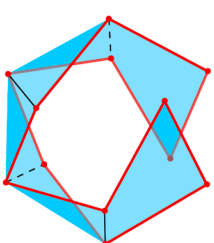
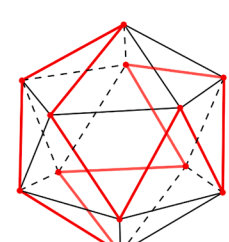
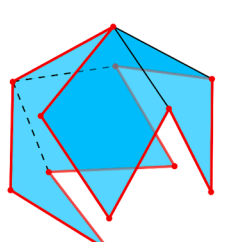
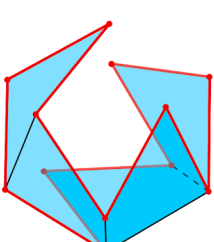
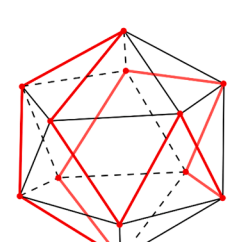
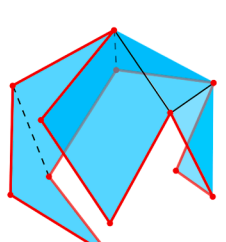
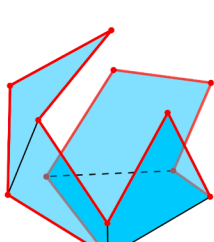
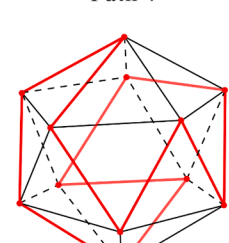
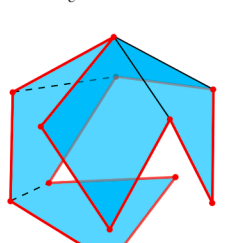
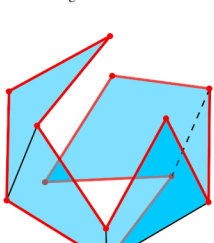
Hamiltonian paths	Two complementary simplest paths	
 <p data-bbox="190 498 259 528">Path 1</p>	 <p data-bbox="521 479 645 508">$c_e=0, c=31$</p>	 <p data-bbox="790 479 914 508">$c_e=0, c=31$</p>
 <p data-bbox="190 787 259 817">Path 2</p>	 <p data-bbox="521 787 645 817">$c_e=0, c=31$</p>	 <p data-bbox="790 787 914 817">$c_e=0, c=31$</p>
 <p data-bbox="190 1075 259 1105">Path 3</p>	 <p data-bbox="521 1075 645 1105">$c_e=0, c=31$</p>	 <p data-bbox="790 1075 914 1105">$c_e=0, c=31$</p>
 <p data-bbox="190 1363 259 1393">Path 4</p>	 <p data-bbox="521 1363 645 1393">$c_e=0, c=31$</p>	 <p data-bbox="790 1363 914 1393">$c_e=0, c=31$</p>
 <p data-bbox="190 1652 259 1681">Path 5</p>	 <p data-bbox="521 1652 645 1681">$c_e=0, c=31$</p>	 <p data-bbox="790 1652 914 1681">$c_e=0, c=31$</p>

Table 2
Reduction results of dodecahedral mechanism using paths 6 to 10.

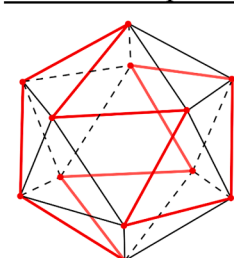
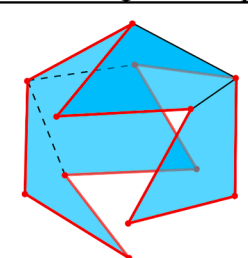
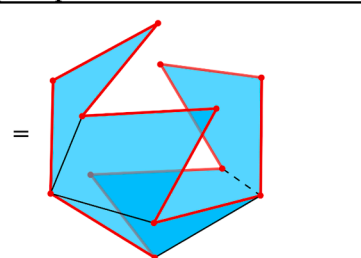
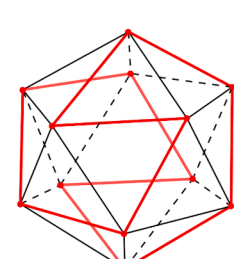
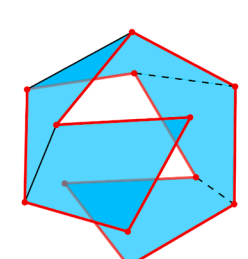
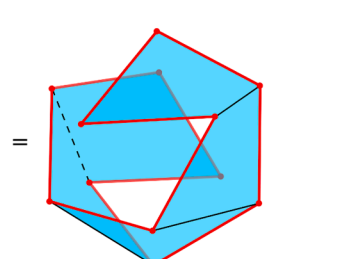
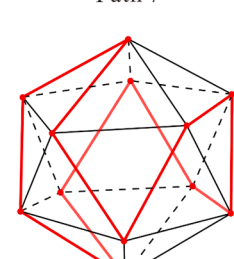
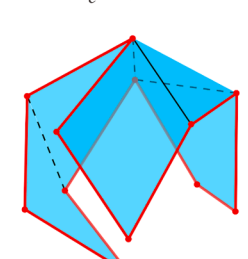
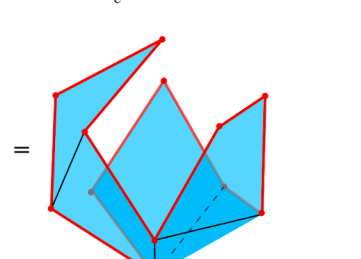
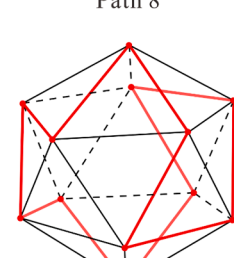
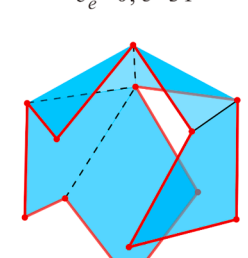
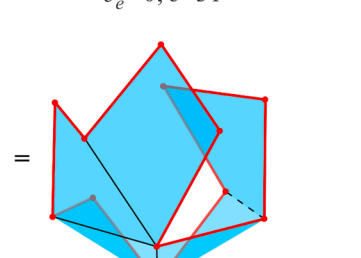
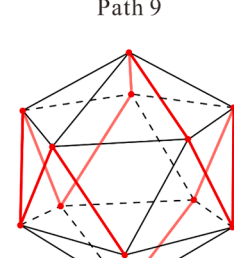
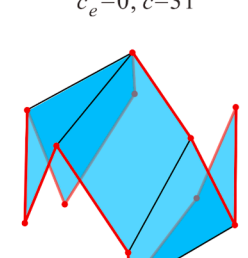
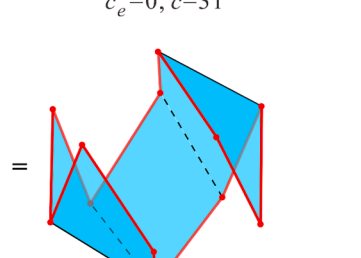
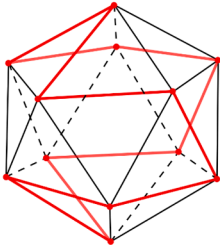
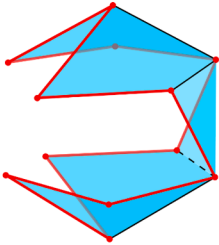
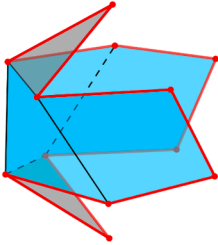
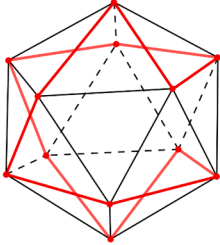
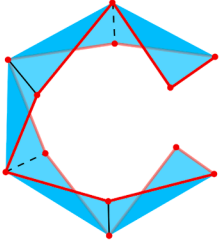
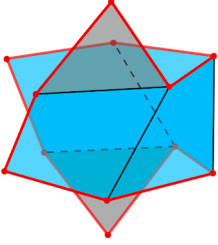
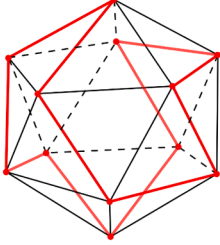
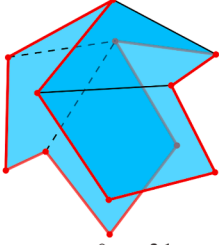
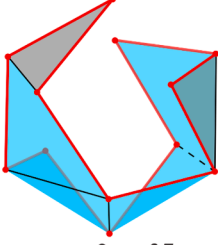
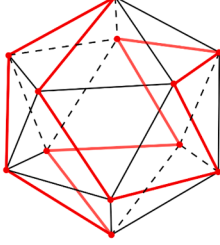
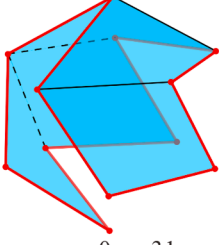
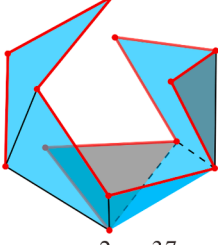
Hamiltonian paths	Two congruent simplest paths	
 <p data-bbox="190 498 263 538">Path 6</p>	 <p data-bbox="511 498 642 538">$c_e=0, c=31$</p>	 <p data-bbox="787 498 918 538">$c_e=0, c=31$</p>
 <p data-bbox="190 797 263 836">Path 7</p>	 <p data-bbox="511 797 642 836">$c_e=0, c=31$</p>	 <p data-bbox="787 797 918 836">$c_e=0, c=31$</p>
 <p data-bbox="190 1095 263 1135">Path 8</p>	 <p data-bbox="511 1095 642 1135">$c_e=0, c=31$</p>	 <p data-bbox="787 1095 918 1135">$c_e=0, c=31$</p>
 <p data-bbox="190 1393 263 1433">Path 9</p>	 <p data-bbox="511 1393 642 1433">$c_e=0, c=31$</p>	 <p data-bbox="787 1393 918 1433">$c_e=0, c=31$</p>
 <p data-bbox="190 1691 263 1775">Path 10</p>	 <p data-bbox="511 1691 642 1775">$c_e=0, c=31$</p>	 <p data-bbox="787 1691 918 1775">$c_e=0, c=31$</p>

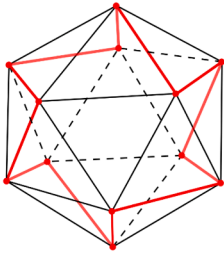
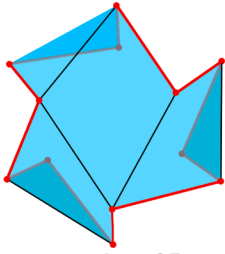
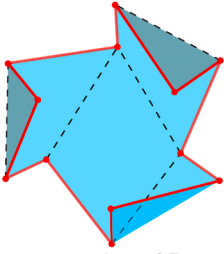
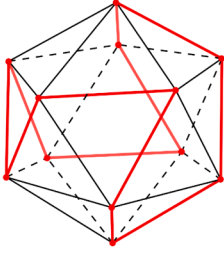
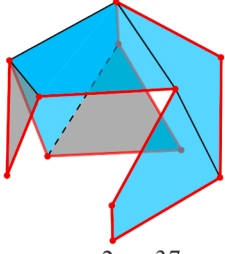
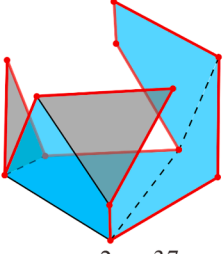
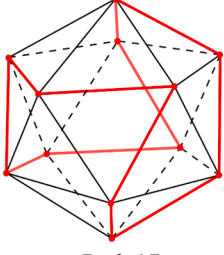
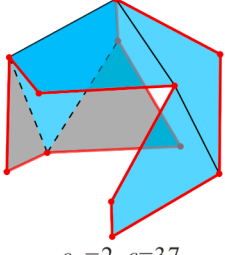
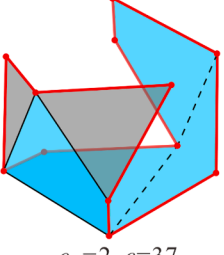
Table 3
Reduction results of dodecahedral mechanism using paths 11 to 14.

Hamiltonian paths	One simplest path and the other non-simplest path	
 Path 11	 $c_e=0, c=31$	 $c_e=2, c=37$
 Path 12	 $c_e=0, c=31$	 $c_e=2, c=37$
 Path 13	 $c_e=0, c=31$	 $c_e=2, c=37$
 Path 14	 $c_e=0, c=31$	 $c_e=2, c=37$

First, similar as the path 1 in Fig. 10(a) which can generate two complementary paths as illustrated in Fig. 10(c) and (e), Table 1 lists five Hamiltonian paths (including path 1) and each one can generate two complementary simplest paths, in which five skew quadrilaterals are still arranged in sequence by sharing four common edges. Next, each Hamiltonian path in Table 2 generates two congruent simplest paths, also as the arrangement of five quadrilaterals, due to its C_2 -symmetry, in which the details of symmetry for each Hamiltonian path can be found in Appendix B [29]. Differently, for two half shells separated from each Hamiltonian path listed in Table 3, one shell can be derived into an effective simplest constraint path as illustrated in blue, the other shell is unsuccessful due to few unmergeable triangular units as illustrated in grey (similar as the case from Fig. 7(b) to 7(c)). The rest three Hamiltonian paths are given in Table 4, yet, from which any effective simplest path can be obtained also as the unmergeable grey triangular units.

Therefore, a total of 19 simplest constraint paths of this dodecahedral mechanism can be found and identified from its 17 Hamiltonian paths, each of which is a sequential arrangement of five skew quadrilateral basic units. As a result, each simplest dodecahedral mechanism can preserve the original one-DOF radial motion behavior and the degrees of overconstraint are greatly

Table 4
Reduction results of dodecahedral mechanism using paths 15 to 17.

Hamiltonian paths	Two non-simplest paths	
 <p>Path 15</p>	 <p>$c_e=2, c=37$</p>	 <p>$c_e=2, c=37$</p>
 <p>Path 16</p>	 <p>$c_e=2, c=37$</p>	 <p>$c_e=2, c=37$</p>
 <p>Path 17</p>	 <p>$c_e=2, c=37$</p>	 <p>$c_e=2, c=37$</p>

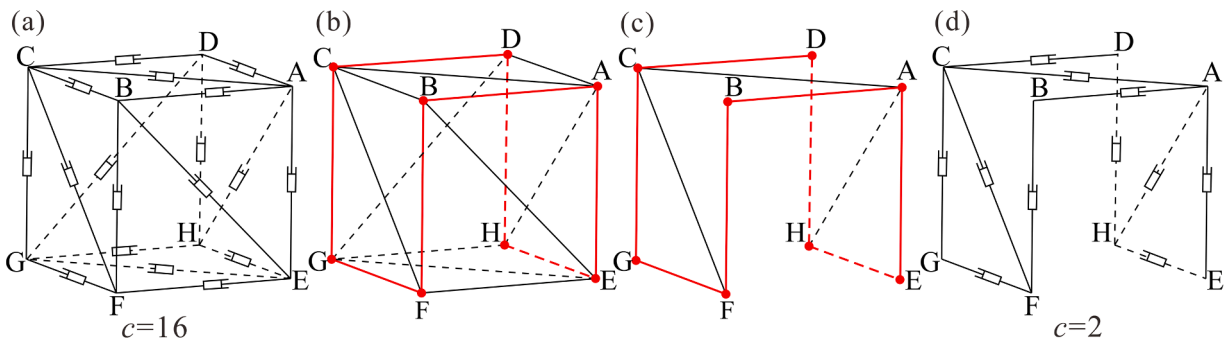


Fig. 13. The reduction of prismatic mechanism with prismatic joints. (a)The original mechanism; (b) the topology graph and its only one Hamiltonian path in red lines; (c) the simplest topology graph; (d) the simplest mechanism. (For interpretation of the references to colour in this figure legend, the reader is referred to the web version of this article.)

reduced from 115 to 31.

3.3. Constraint reduction of a prismatic-based deployable polyhedral mechanism

Furthermore, the reduction method proposed in this paper can be readily applied into the expanding structures constructed by prismatic joints. A quadrangular-prism mechanism is created in Fig. 13(a) as an example based on the construction approach in [30], in which all the quadrangular faces have been triangulated to generate the one-DOF motion. Based on the original mechanism in Fig. 13(a) with 8 rigid links A to H, 12 prismatic joints and overconstraints $c = 16$, the corresponding mechanism topology graph is illustrated in Fig. 13(b), in which its only one Hamiltonian path is highlighted by red lines [29]. Next, two congruent half shells can be split by this Hamiltonian path due to the symmetry, we further remove BC and AD in the resulted half shell following the proposed reduction method and topology operation, its simplest topology graph is obtained and demonstrated in Fig. 13(c). In addition to skew quadrilateral units ABFC and ACDH, there are two triangular units GFC and AEH should be reserved under reduction premise, in which any line cannot be further removed. Finally, by mapping this simplest topology to prismatic mechanism, the simplest quadrangular-prism mechanism is shown in Fig. 13(d), in which the overconstraints are reduced from 16 to 2, and it can be found that the original radial motion is still preserved.

4. Conclusions

In this paper, we proposed a novel Hamiltonian-path based constraint-reduction method for a family of one-DOF Sarrus-inspired DPMs. By introducing Hamiltonian paths on 3D topological graphs, constraint reduction strategy for the multi-loop overconstrained DPMs was proposed based on skew quadrilateral basic units and their sequential arrangements. All Hamiltonian paths on their dual tetrahedron, octahedron and icosahedron were detailedly discussed to obtain one simplest tetrahedral mechanism, one simplest cubic mechanism and nineteen dodecahedral mechanisms, respectively. The degree of overconstraint in each simplest DPM is greatly reduced while preserving original motion behavior, i.e., one-DOF synchronized radial motion.

Referring to the proposed approach, the simplified form (non-simplest form) of multi-loop polyhedral mechanisms can also be selected and obtained for the specific applications, such as the deployable structures that need appropriate actuation and stiffness without affecting the kinematics. Yet, after mapping the simplest topology to the original mechanism constructed by Sarrus linkages, the degrees of overconstraint are still exist due to the overconstrained construction element, future work will explore the non-overconstrained assembly of spatial linkages, such as spatial 7R or 8R linkages. Synthesis and reduction process of the Sarrus-inspired mechanisms were presented in this paper, which could provide inspirations for the deduction of the known multiloop mechanisms or the construction of new ones with less or even no overconstraint, with potential applications in the fields of manufacturing, architecture and space exploration.

Declaration of Competing Interest

The authors declare that they have no known competing financial interests or personal relationships that could have appeared to influence the work reported in this paper.

Data availability

No data was used for the research described in the article.

Acknowledgements

Y.C. acknowledged the support of the National Natural Science Foundation of China (Projects 52320105005, 52035008, 51825503) and the New Cornerstone Science Foundation through the XPLOER PRIZE (XPLOER-2020-1035). X. Z. acknowledges financial support from the Natural Science Foundation of China (Project No. 52105032).

Appendix A

According to the original tetrahedral mechanism and its kinematic solution [16] based on D-H matrix method [31], the simplified tetrahedral mechanism and the simplest form are illustrated in Fig. A1(a) and (b), respectively. Meanwhile, $\varphi'_i = 2\varphi_i$ still exist in all involved Sarrus linkages, yet some original 9R linkages are vanished after reduction. First, a spatial 12R linkage with revolute axes z_1 to z_{12} can be identified in Fig. A1(a) after removing the Sarrus linkage between platforms B and C, respectively, its motion constraint conditions can be obtained as follows, among platforms A, D and B,

$$\varphi_1 = \varphi_2 = \varphi_3, \varphi'_1 = \varphi'_2 = \varphi'_3, \quad (A1)$$

among platforms A, D and C,

$$\varphi_3 = \varphi_2 = \varphi_6, \varphi'_3 = \varphi'_2 = \varphi'_6. \tag{A2}$$

Substituting this constraint conditions into matrix calculations of this 12R linkage yields

$$\varphi_1 = \varphi_2 = \varphi_3 = \varphi_5 = \varphi_6, \varphi'_1 = \varphi'_2 = \varphi'_3 = \varphi'_5 = \varphi'_6. \tag{A3}$$

Thus, the identical kinematic behavior of five involved Sarrus linkages and the equivalent kinematics of the entire simplified tetrahedral mechanism are revealed.

On the other hand, there are no original 9R linkages reserved in the simplest mechanism in Fig. A1(b), thus the constraint conditions in Eqs. (A1) and (A2) no longer exist, we can only utilize the fundamental conditions in each Sarrus linkage, i.e.,

$$\varphi'_1 = 2\varphi_1, \varphi'_3 = 2\varphi_3, \varphi'_5 = 2\varphi_5, \varphi'_6 = 2\varphi_6, \tag{A4}$$

after the matrix calculations of this 12R linkage, we have

$$\varphi_1 = \varphi_3 = \varphi_5 = \varphi_6, \varphi'_1 = \varphi'_3 = \varphi'_5 = \varphi'_6. \tag{A5}$$

Therefore, the equivalent kinematics of four involved Sarrus linkages and the entire simplest tetrahedron can also be obtained.

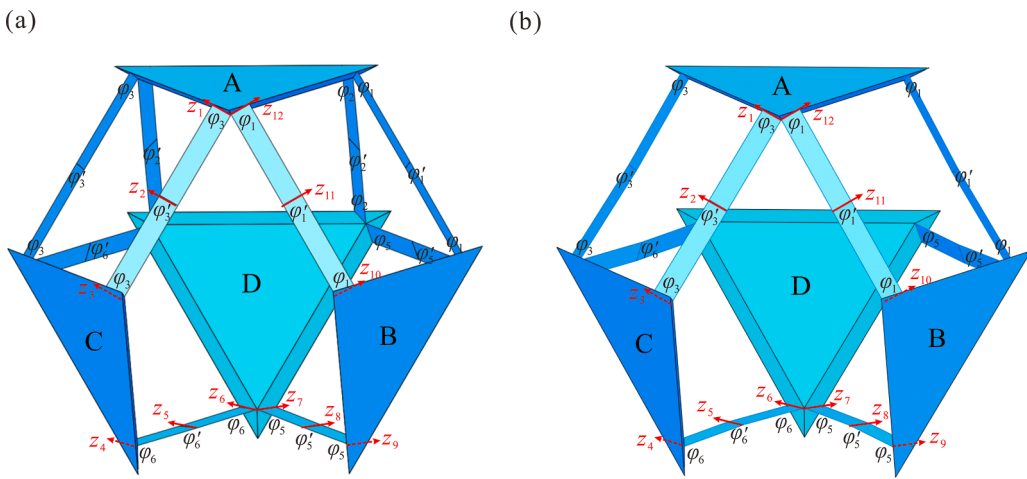


Fig. A1. Analysis of kinematic variables in (a) the simplified tetrahedral mechanism and (b) its simplest one.

Appendix B

Taking the Hamiltonian path 2 with C_2 -symmetry in an icosahedron (given in Table 1) as an example, as shown in Fig. B1(a), it has a rotational symmetry C_2 -axis (highlighted in blue), this path can be rotated 180° around the C_2 -axis then coincide with itself, in which the mentioned rotational symmetry only refers to the red-line path. Next, two distinct half shells, shell 2.1 and shell 2.2, split by path 2 are illustrated in Fig. B1(b) and (d). Based on the C_2 -symmetry, shell 2.1 also can coincide with itself after 180° rotation around the C_2 -axis, see Fig. B1(c), although the blue facets inside the red path rotate together with the path, so do the shell 2.2 in Fig. B1(d) and (e) before and after 180° rotation.

On the other hand, Hamiltonian path 6 (given in Table 2) also has the C_2 -symmetry referring to red lines as shown in Fig. B1(a), it split an icosahedron into two identical shells, shell 6.1 and shell 6.2, both of which has the original C_2 -symmetry including the inside blue facets. Differently, after the 180° rotation, shell 6.1 becomes the shell 6.2, and vice versa, see Fig. B2(b) to (d). Hence, we call them two congruent shells, and this rotational symmetry is named as C_2 -symmetry' to distinguish from the similar case given in Fig. B1.

In summary, the details of symmetry for all 17 Hamiltonian paths are listed in Fig. B3, besides the C_2 -symmetry, there are several paths without any symmetry. Especially, path 15 has a C_3 -symmetry, meaning that it can coincide with itself after 120° or 240° rotation around C_3 -axis.

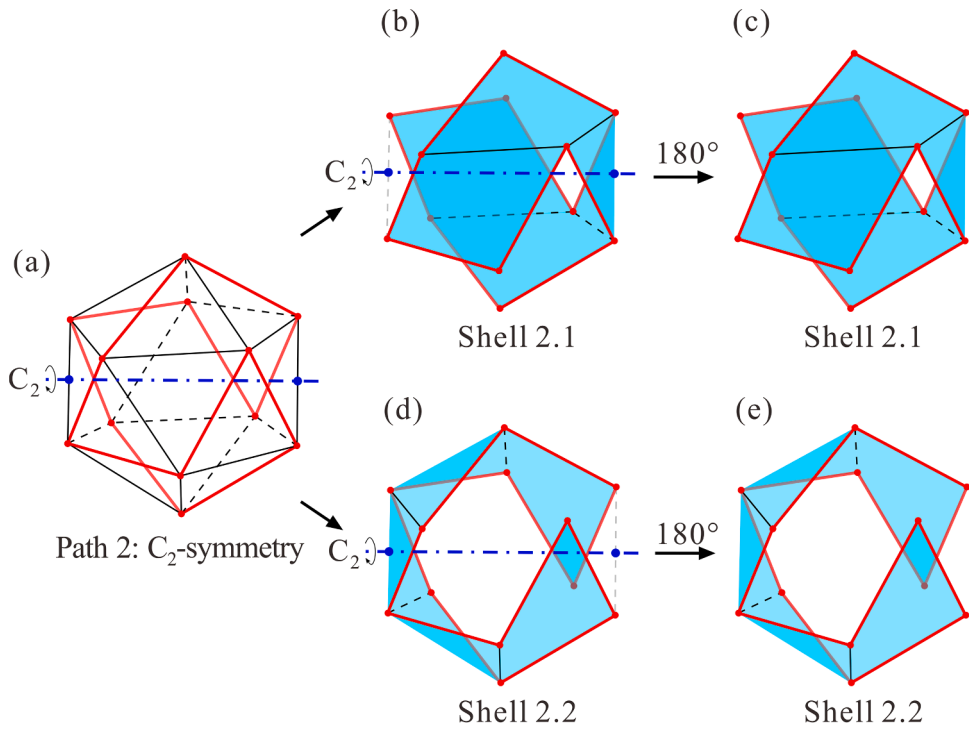


Fig. B1. C_2 -symmetry in the Hamiltonian path 2.

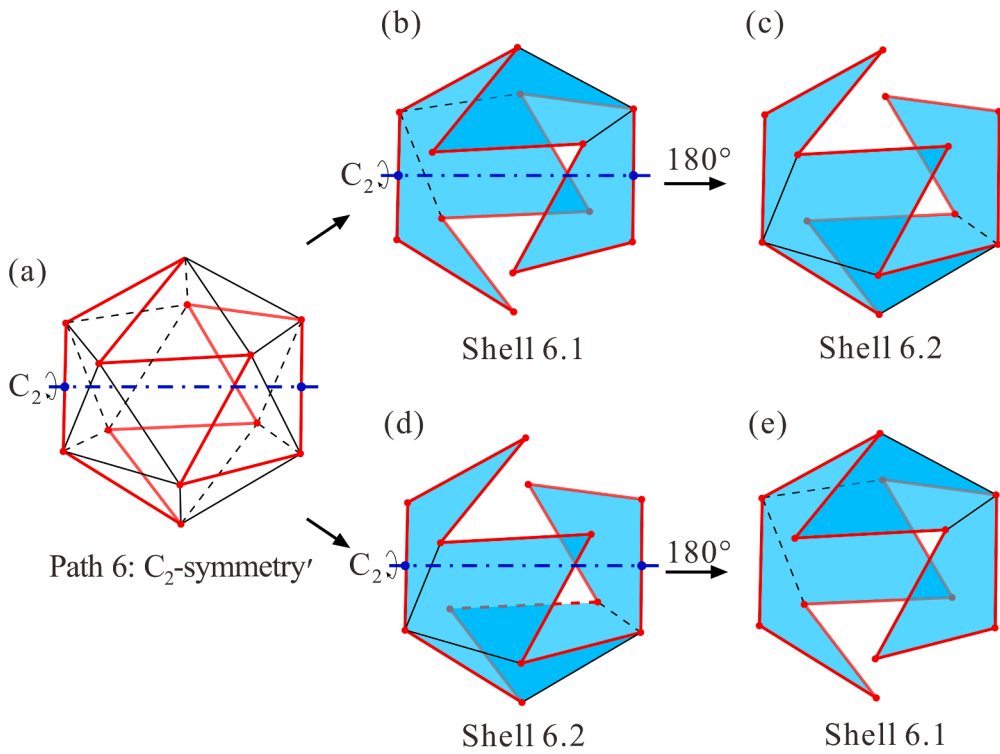


Fig. B2. C_2 -symmetry' in the Hamiltonian path 6.

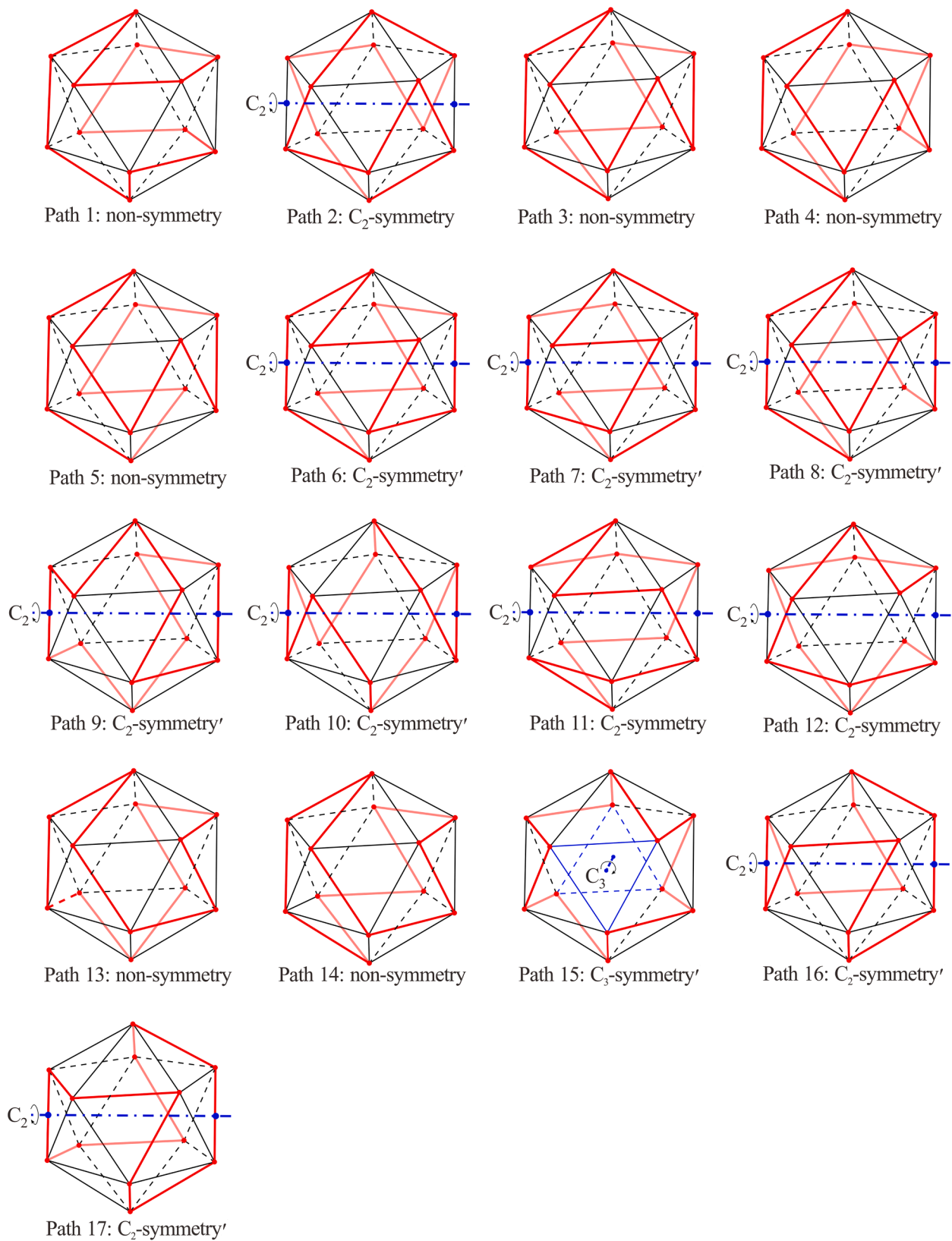


Fig. B3. Symmetries in different Hamiltonian paths.

References

- [1] Y. Gu, X. Zhang, G. Wei, Y. Chen, Sarrus-Inspired Deployable Polyhedral Mechanisms, 2308, arXiv, 2023, p. 15874. <http://arxiv.org/abs/2308.15874>.
- [2] G. Wei, J.S. Dai, A spatial eight-bar linkage and its association with the deployable platonic mechanisms, *J. Mech. Robot.* 6 (2014), 021010.
- [3] G. Wei, Y. Chen, J.S. Dai, Synthesis, mobility, and multifurcation of deployable polyhedral mechanisms with radially reciprocating motion, *J. Mech. Des.* 136 (2014), 091003.
- [4] G. Wei, Geometric Analysis and Theoretical Development of Deployable Polyhedral Mechanisms. PhD thesis, King's College London, United Kingdom, 2011.
- [5] H. Guo, J. Zhang, R. Liu, Z. Deng, Effects of joint on dynamics of space deployable structure, *Chin. J. Mech. Eng.* 26 (2013) 861–872.
- [6] X. Zhang, R. Nie, Y. Chen, B. He, Deployable structures: structural design and static/dynamic analysis, *J. Elast* 146 (2021) 199–235.
- [7] K. Wohlhart, Kinematics and dynamics of the fulleroid, *Multibody Syst Dyn* 1 (1997) 241–258.
- [8] H. Xiu, A “double V-shaped” eightbar linkage and its associated Fulleroid-like DPMS and application, PhD thesis, Jilin University, China, 2019.
- [9] G. Wei, J.S. Dai, Origami-inspired integrated planar-spherical overconstrained mechanisms, *J. Mech. Des.* 136 (2014), 051003.
- [10] Y. Zhang, M. Li, Y. Chen, R. Peng, X. Zhang, Thick-panel origami-based parabolic cylindrical antenna, *Mech. Mach. Theory* 182 (2023), 105233.
- [11] J. Liu, Y. Xu, Y. Liu, H. Shi, X. Jiang, Configuration design of single-loop non-overconstrained mechanism with inactive joints, *Iran. J. Sci. Technol. Trans. Mech. Eng.* 46 (2020) 1–9.
- [12] J. Qi, Y. Gao, F. Yang, Synthesis of clearance for a kinematic pair to prevent an overconstrained linkage from becoming stuck, *Mech. Sci.* 14 (1) (2023) 171–178.
- [13] M. Wojtyra, Joint reaction forces in multibody systems with redundant constraints, *Multibody Syst. Dyn.* 14 (2005) 23–46.
- [14] M. Wojtyra, J. Frączek, Comparison of selected methods of handling redundant constraints in multibody systems simulations, *ASME J. Comput. Nonlinear Dyn.* 8 (2) (2013), 021007.
- [15] P. Milenkovic, M.V. Brown, Properties of the Bennett mechanism derived from the RRRS closure ellipse, *J. Mech. Robot.* 3 (2011), 021012.
- [16] C.C. Lee, J.M. Hervé, Oblique circular torus, villarceau circles and four types of Bennett linkages, *Proc. Inst. Mech. Eng. Part C* 228 (2011) 742–752.
- [17] F. Yang, Y. Chen, R. Kang, J. Ma, Truss transformation method to obtain the non-overconstrained forms of 3D overconstrained linkages, *Mech. Mach. Theory* 102 (2016) 149–166.
- [18] J.C. Maxwell, On the calculation of the equilibrium and stiffness of frames, *Lond. Edinburgh Dublin Philos. Magaz. J. Sci.* 27 (1864) 294–299.
- [19] N. Brown, C. Ynchausti, A. Lytle, L.L. Howell, S.P. Magleby, Approaches for minimizing joints in single-degree-of-freedom origami-based mechanisms, *J. Mech. Des.* 144 (2022), 103301.
- [20] D. Bolanos, C. Ynchausti, N. Brown, H. Pruett, J. Hunter, B. Clark, T. Bateman, L.L. Howell, S.P. Magleby, Considering thickness-accommodation, nesting, grounding and deployment in design of Miura-oribased space arrays, *Mech. Mach. Theory* 174 (2022), 104904.
- [21] X. Zhang, Study On the Relationship Between Mobile Assemblies of Spatial Linkages and Rigid Origami, Tianjin University, 2018.
- [22] Y. Chen, R. Peng, Z. You, Origami of thick panels, *Science* 349 (2015) 396–400.
- [23] X. Zhang, Y. Chen, Mobile assemblies of Bennett linkages from four-crease origami patterns, *Proc. R. Soc. A* 474 (2018), 20170621.
- [24] X. Zhang, Y. Chen, The diamond thick-panel origami and the corresponding mobile assemblies of plane-symmetric bricard linkages, *Mech. Mach. Theory* 130 (2018) 585–604.
- [25] J. Yang, X. Zhang, Y. Chen, Z. You, Folding arrays of uniform-thickness panels to compact bundles with a single degree of freedom, *Proc. R. Soc. A* 478 (2022), 20220043.
- [26] C.H. Séquin, Symmetrical Hamiltonian manifolds On Regular 3D and 4D Polytopes, *Renaissance Banff: Mathematics, Music, Art, Culture*, 2005, pp. 463–472.
- [27] K.H. Hunt, Kinematic Geometry of Mechanisms, Oxford University Press, Clarendon, Oxford, UK, 1978.
- [28] H. Heesch, *Gesammelte Abhandlungen*, Verlag Barbara Franzbecker, 1986.
- [29] F. Effenberger, W.J.D. Kühnel, Hamiltonian submanifolds of regular polytopes, *Discrete Comput. Geom.* 43 (2010) 242–262.
- [30] S.K. Agrawal, S. Kumar, M. Yim, Polyhedral single degree-of-freedom expanding structures: design and prototypes, *J. Mech. Des.* 124 (2002) 473–478.
- [31] J. Denavit, R.S. Hartenberg, A kinematic notation for lower-pair mechanisms based on matrices, *Trans. ASME J. Appl. Mech.* 22 (1955) 215–221.